1-23-2017

Characterizing Substrate–Surface Interactions on Alumina-Supported Metal Catalysts by Dynamic Nuclear Polarization-Enhanced Double-Resonance NMR Spectroscopy

Frédéric A. Perras
Ames Laboratory, fperras@ameslab.gov

J. Daniel Padmos
Queen's University

Robert L. Johnson
Iowa State University

Lin-Lin Wang
Ames Laboratory, llw@ameslab.gov

Thomas J. Schwartz
University of Wisconsin-Madison

See next page for additional authors

Characterizing Substrate–Surface Interactions on Alumina-Supported Metal Catalysts by Dynamic Nuclear Polarization-Enhanced Double-Resonance NMR Spectroscopy

Abstract

The characterization of nanometer-scale interactions between carbon-containing substrates and alumina surfaces is of paramount importance to industrial and academic catalysis applications, but it is also very challenging. Here, we demonstrate that dynamic nuclear polarization surface-enhanced NMR spectroscopy (DNP SENS) allows the unambiguous description of the coordination geometries and conformations of the substrates at the alumina surface through high-resolution measurements of 13C–27Al distances. We apply this new technique to elucidate the molecular-level geometry of 13C-enriched methionine and natural abundance poly(vinyl alcohol) adsorbed on γ-Al2O3-supported Pd catalysts, and we support these results with element-specific X-ray absorption near-edge measurements. This work clearly demonstrates a surprising bimodal coordination of methionine at the Pd–Al2O3 interface.

Disciplines

Chemical Engineering | Materials Chemistry | Materials Science and Engineering

Comments

This document is the Accepted Manuscript version of a Published Work that appeared in final form in the *Journal of the American Chemical Society*, copyright © American Chemical Society after peer review and technical editing by the publisher. To access the final edited and published work see 10.1021/jacs.6b11408. Posted with permission.

Authors

Frédéric A. Perras, J. Daniel Padmos, Robert L. Johnson, Lin-Lin Wang, Thomas J. Schwartz, Takeshi Kobayashi, J. Hugh Horton, James A. Dumesic, Brent H. Shanks, Duane D. Johnson, and Marek Pruski

Characterizing Substrate-Surface Interactions on Alumina-Supported Metal Catalysts by DNP-Enhanced Double-Resonance NMR Spectroscopy

Frédéric A. Perras,[a] J. Daniel Padmos,[b] Robert L. Johnson,[c] Lin-Lin Wang,[a] Thomas J. Schwartz,[d†] Takeshi Kobayashi,[a] J. Hugh Horton,[b] James A. Dumesic,[d] Brent H. Shanks,[c] Duane D. Johnson,[a,c,e] Marek Pruski*[a,f]

[a] US DOE, Ames Laboratory, Ames, IA, 50011, USA

[b] Department of Chemistry, Queen's University, Kingston, ON K7L 3N6, Canada

[c] Department of Chemical and Biological Engineering, Iowa State University, Ames, IA 50011, USA

[d] Department of Chemical and Biological Engineering, University of Wisconsin, Madison, WI, 53706, USA

[e] Department of Materials Science and Engineering, Iowa State University, Ames, IA, 50011, USA

[f] Department of Chemistry, Iowa State University, Ames, IA, 50011, USA

ABSTRACT

The characterization of nanometer-scale interactions between carbon-containing substrates and alumina surfaces is of paramount importance to industrial and academic catalysis applications, but it is also very challenging. Here, we demonstrate that dynamic nuclear polarization surface-enhanced NMR spectroscopy (DNP SENS) allows the unambiguous description of the coordination geometries and conformations of the substrates at the alumina surface through high-resolution measurements of ^{13}C-^{27}Al distances. We apply this new technique to elucidate the molecular-level geometry of ^{13}C-enriched methionine and natural abundance poly(vinyl alcohol) adsorbed on γ-Al_2O_3-supported Pd catalysts, and support these results with element-specific X-ray absorption near edge measurements. This work clearly demonstrates a surprising bimodal coordination of methionine at the Pd-Al_2O_3 interface.

INTRODUCTION

Dynamic nuclear polarization (DNP) has recently provided a revolutionary means for increasing the sensitivity of solid-state (SS)NMR experiments performed on surfaces, using an approach termed DNP surface-enhanced NMR spectroscopy (SENS).[1] In DNP SENS, the NMR response from surface adsorbates is boosted by a microwave-induced polarization transfer from the unpaired electrons of exogenously introduced radical dopants. This transfer hyperpolarizes the ^{1}H spins situated at the surface providing theoretical sensitivity enhancements as large as $\gamma_e/\gamma_H = 658$ and enabling previously inconceivable means for atomic-scale characterizations of surfaces and interfaces.[2]

DNP SENS has had an especially high impact on the characterization of silica-supported heterogeneous catalytic systems. The increase in sensitivity has enabled the rapid acquisition of 1D and 2D SSNMR spectra of silica surface species and catalysts, which, in particular, afforded "indirect" Si-C proximity information through independent $^{13}C\{^{1}H\}$ and $^{29}Si\{^{1}H\}$ correlation experiments. These studies have generated in-depth knowledge about the structures, conformations and chemical activities of these species needed for rational design and synthesis of improved silica-based catalysts.[3]

The application of DNP SENS to similarly characterize alumina-supported heterogeneous catalysts is very desirable. Gamma-alumina (γ-Al_2O_3) is one of the most important, and the most common, catalyst supports used by the petrochemical industry,[4] due to its low cost, high surface area, large pore size, and high thermochemical stability, as well as the presence of Lewis acidity. These properties also enable the synthesis of γ-Al_2O_3-supported metal catalysts with high metal dispersions. Some of the most industrially significant applications of such catalysts include vehicle catalytic converters and the processing of petroleum.[4] Clearly, gaining the atomic-scale

understanding of the alumina-supported metal catalysts' surface structures by DNP SENS would accelerate the structure-driven development of new catalytic materials, much like the work that has been done on silica-supported catalysts. While pure alumina samples have been studied by DNP,[5] this field is largely unexplored.

We recently applied ^{13}C DNP SENS to characterize the degradation products of methionine on a Pd/γ-Al_2O_3 catalyst.[6] Methionine is a common impurity found in biological feedstocks, and is a strong inhibitor of reduced metal catalysts.[7] Our *post-mortem* studies were able to determine the pathways and adsorbates that lead to catalyst deactivation. ^{13}C NMR experiments, however, yield minimal information regarding the location of these adsorbates at the surface. Here, we demonstrate the use of DNP-enhanced double-resonance $^{13}C\{^{27}Al\}$ experiments, in concert with X-ray absorption near edge structure (XANES) measurements and DFT calculations, to obtain precise locational and conformational information about ^{13}C-enriched methionine as well as natural abundance poly(vinyl alcohol) (PVA) adsorbed on γ-Al_2O_3-supported Pd catalysts to prevent deactivation. Although the low surface loadings prevented the use of such experiments in the past, the added dimension to structural characterization offered by DNP SENS opens new horizons for the design, evaluation and development of alumina-supported metal catalysts, so frequently used in industrial catalysis.

MATERIALS AND METHODS

Catalyst Synthesis. The synthesis of Pd/γ-Al_2O_3 catalysts (both with and without PVA) was described previously.[7] Briefly, the parent Pd/γ-Al_2O_3 catalyst was prepared by loading $Pd(NO_3)_2$ (using Aldrich 10% $Pd(NO_3)_2$ solution in 10% HNO_3, 99.999%) onto γ-Al_2O_3 (Strem, low-soda) by incipient wetness impregnation. The catalyst was subsequently dried in air at 383 K for 2 hours, calcined in flowing air at 673 K, reduced in flowing dihydrogen at 533 K, and passivated

with 1% O_2 in Ar. The PVA-impregnated catalyst was prepared in the dark (to prevent premature cross-linking) by incipient wetness impregnation of PVA (Aldrich, 99+% hydrolyzed, 89,000-98,000 amu) and benzoyl peroxide (Luperox A98, ≥98%), both dissolved in a 50 wt% mixture of THF (Fisher Scientific, Certified) and Milli-Q grade water (≤18 MΩ·cm), into the parent Pd/γ-Al_2O_3 catalyst. The catalyst was then dried under vacuum in the dark at 313 K for 2 hours, cross-linked under UV light at 365 nm, and washed by Soxhlet extraction with 1-butanol. Finally, the catalyst was rinsed with Milli-Q grade water and dried under vacuum at 313 K. The γ-Al_2O_3, Pd/γ-Al_2O_3, and PVA-impregnated Pd/γ-Al_2O_3 catalysts have been characterized in our earlier studies by CO chemisorption, N_2 physisorption, transmission electron microscopy (TEM), and S 2p X-ray photoelectron spectroscopy (XPS).[6,7] The results from these measurements will be summarized later in the text.

Prior to performing NMR measurements, the catalyst samples were loaded with uniformly or selectively ^{13}C-enriched methionine (Cambridge Isotope Laboratories; L-methionine U-13C5 97-99%) by incipient wetness impregnation as described previously.[6] Briefly, methionine was added to the reduced and passivated Pd/γ-Al_2O_3, PVA-impregnated Pd/γ-Al_2O_3, and γ-Al_2O_3 materials by incipient wetness impregnation using solutions in D_2O (Aldrich, 99.0 atom% D). The samples were dried under vacuum at 318 K. The methionine coverages used were 94 μmol g^{-1} in both the Pd-free and Pd-containing materials, which corresponds to ~0.3 molecules per nm^2 of surface.

X-Ray Absorption Near Edge Structure (XANES). Sulfur K-edge and Pd L_3-edge XANES experiments were conducted at the soft X-ray microcharacterization beamline (SXRMB, 06B1-1, Canadian Light Source, Saskatoon, SK, Canada). The powdered samples were first dispersed onto double-sided carbon tape which was affixed to a sample holder plate. The sample plate was

then mounted inside the chamber at a 45° angle to the incident X-ray beam and allowed to reach ultra-high vacuum before the measurements. For the S K-edge measurements, S K_α fluorescence was measured in the range of 2430–2520 eV with a four-element silicon drift detector, while for Pd L_3-edge, the total electron yield was measured in the range of 3130–3210 eV. All of the XANES spectra were processed with Athena, part of the IFEFFIT software package.[8]

SSNMR. *Bruker AVANCE III 400 DNP NMR Spectrometer*. All DNP SSNMR experiments were performed on a commercial Bruker AVANCE III 400 DNP NMR spectrometer equipped with a 263 GHz gyrotron and a 3.2-mm low-temperature MAS probe. The samples were impregnated with a 16 mM solution of TEKPol,[9] which was purchased from Aix Marseille, in 1,1,2,2-tetrachloroethane (TCE) and packed into the sapphire rotors. The rotors were sealed with a Teflon insert and pre-spun at room temperature prior to performing the DNP SSNMR experiments at 105 K. The spinning frequency was set to 10 kHz for all DNP SSNMR experiments.

1D ^{13}C cross-polarization (CP)MAS experiments were performed using a 2.1 μs ^{1}H excitation pulse, a 2 ms contact time, and 128 scans with a 6 s recycle delay. ^{27}Al PRESTO-III[10] (phase-shifted recoupling effects a smooth transfer of polarization) experiments were performed using four equal $R18_1^7$ recoupling periods of 200 μs, along with 5 and 10 μs central transition-selective ^{27}Al 90° and 180° pulses, respectively. The recycle delay was set to 4 s, and 128 scans were acquired. The DNP enhancement factors (ε) were measured by acquiring the ^{13}C and ^{27}Al SSNMR spectra with the microwaves turned on and off; they are listed in Table 1.

2D ^{27}Al{^{1}H} PRESTO-III frequency-switched-Lee-Goldburg (FSLG) heteronuclear correlation (HETCOR) experiments were performed using the same pulse parameters as the 1D PRESTO-III experiments. FSLG homonuclear decoupling[11] was applied to improve the ^{1}H

resolution and 16 t_1 increments of 78.67 μs, each consisting of 32 scans, were acquired. The States-TPPI procedure was used to obtain purely absorptive 2D spectra. In an attempt to observe longer range correlations, a second HETCOR spectrum was also acquired using cross-polarization. The contact time was set to 1 ms and 94 t_1 increments, each consisting of 64 scans, were acquired.

The $^{13}C\{^{27}Al\}$ rotational-echo saturation pulse double-resonance (RESPDOR) experiments were performed using a REDOR box purchased from NMR-service. CP parameters identical to those listed above were used, along with a 10 μs ^{13}C refocusing pulse. The SFAM-1 recoupling scheme[12] was used with a 30 kHz frequency sweep and a 30 kHz ^{13}C RF field strength. The use of SFAM-2, which in addition decouples ^{13}C-^{13}C homonuclear dipolar coupling interactions, was also evaluated and led to consistent results. SFAM-1 was chosen in the end due to its larger scaling factor enabling longer distances to be measured.[13] ^{13}C spectra with varying recoupling times (t_{rec}) were acquired with (S) and without (S_0) the application of two 75 μs 110 kHz ^{27}Al saturation pulses situated symmetrically on either side of the ^{13}C refocusing pulse. The recoupling curves were obtained by plotting $\Delta S/S_0$ for each ^{13}C resonance as a function of the recoupling time and were fitted using an in-house C program described below.

Bruker AVANCE II 600 NMR spectrometer. Conventional ^{13}C SSNMR experiments on Pd/γ-Al_2O_3 samples impregnated with varying amounts of $^{13}CH_3$-methionine were acquired at field strength of 14.1 T using a Bruker AVANCE II 600 NMR spectrometer. The samples were packed into 4-mm rotors and spun at 7 kHz. We used a spin echo sequence with 90° and 180° pulse durations of 4 and 8 μs, respectively, and a total of 1024 scans were accumulated with a recycle delay of 2 s.

Varian NMR System 600 MHz NMR spectrometer. The 2D $^{1}H\{^{27}Al\}$ DFS-CP-HETCOR experiment was performed on a Varian 600 MHz NMR system using a 1.6-mm fast MAS probe. The ^{27}Al central-transition polarization was enhanced by a 2.5 ms double-frequency sweep (DFS) pulse,[14] sweeping from ±500 kHz to ±50 kHz. A 20 μs central-transition selective 90° pulse was then applied to the aluminum, and the polarization was transferred to ^{1}H using a 15 ms CP contact time, following the t_1 evolution period. A total of 32 t_1 increments of 50 μs each were acquired and the States-TPPI procedure was used to obtain purely absorptive phase 2D lineshapes.

Density Functional Theory (DFT) Calculations. Methionine chemisorption on a Pd_{13} cluster (see Figure S1 in Supporting Information) was studied with DFT,[15] using the generalized gradient approximation (GGA) of Perdew, Burke, and Ernzerhof (PBE)[16] in a plane-wave basis set with projector augmented waves,[17] as implemented in the Vienna *Ab-initio* Simulation Package (VASP).[18] Chemical shifts were calculated using a linear-response method.[19] The methionine-Pd_{13} cluster was placed in a 15 Å cubic box and all atoms were relaxed until the absolute values of the forces were below 0.02 eV/Å. A kinetic energy cutoff of 400 eV for the plane-wave basis set and a Γ Monkhorst-pack[20] *k*-point mesh were used for this cell.

RESULTS AND DISCUSSION

Catalyst Characterization. Previously, we performed CO chemisorption and N_2 physisorption measurements to characterize the same γ-Al_2O_3, Pd/γ-Al_2O_3, and PVA/Pd/γ-Al_2O_3 catalysts as those used here.[7] For the 2% Pd/γ-Al_2O_3 sample, the CO uptake measurement was 63 μmol g^{-1}, which leads to a dispersion of 50%, assuming a CO-Pd stoichiometry of 0.67.[7] For spherical nanoparticles, the nanoparticle diameter (d) is related to the metal dispersion (D) by the relation d=1.1/D, indicating the surface-averaged Pd nanoparticle size is 2.2 nm for this sample. The

average CO uptake decreases to 38 μmol g^{-1} following PVA intercalation, although TEM micrographs and ICP-AES analysis in our previous work show that such decreases correspond to site-blocking by PVA rather than an increase in the metal nanoparticle size.[7] Intercalation with PVA also causes a decrease in the pore diameter, from 7 nm for the Pd/γ-Al_2O_3 catalyst to 6 nm for the PVA/Pd/γ-Al_2O_3 catalyst.[7] In our previous work, we concluded that the decreases in both CO uptake and pore size following intercalation are due to a coating of PVA that is formed on the inside of the pore walls of the γ-Al_2O_3 support.

^{13}C MAS SSNMR spectroscopy. We have investigated the impregnation of methionine on supported Pd catalysts by ^{13}C MAS SSNMR spectroscopy (Figure 1 and Table S1). The bottom spectrum in Figure 1 represents uniformly-^{13}C-enriched methionine on pure γ-Al_2O_3, with the peaks at 31 ppm and 13 ppm corresponding to the methylene and methyl resonances, respectively. As can be seen in the spectra of Pd/γ-Al_2O_3 catalysts (Figure 1b-d), this time impregnated with selectively $^{13}CH_3$-enriched methionine, a significant chemical shift change (to 19 ppm) and broadening of the methylene resonance occurs in the presence of Pd.[6b] A shoulder also appears at 22 ppm from dissociated, Pd-bound, SCH_3.[6b] Previous DNP-enhanced ^{13}C homonuclear correlation experiments have confirmed that methionine retains its structure and that the shift cannot be caused by a chemical reaction.[6a] Additionally, it can be seen that this change in chemical shift is not due to a susceptibility effect; if more methionine is impregnated than there are available surface Pd binding sites (as determined by CO chemisorption), a second resonance at 13 ppm appears (Figure 1c), which, as previously stated, corresponds to methionine adsorbed onto the alumina surface. Further saturation leads to the crystallization of α- and β-methionine outside of the support (Figure 1d).[21] The positive resonance shift of 6 ppm must then

originate from the coordination of the methionine S atom with the Pd nanoparticle surface.[6,7] This assignment is further supported by DFT calculations and XANES measurements, *vide infra*.

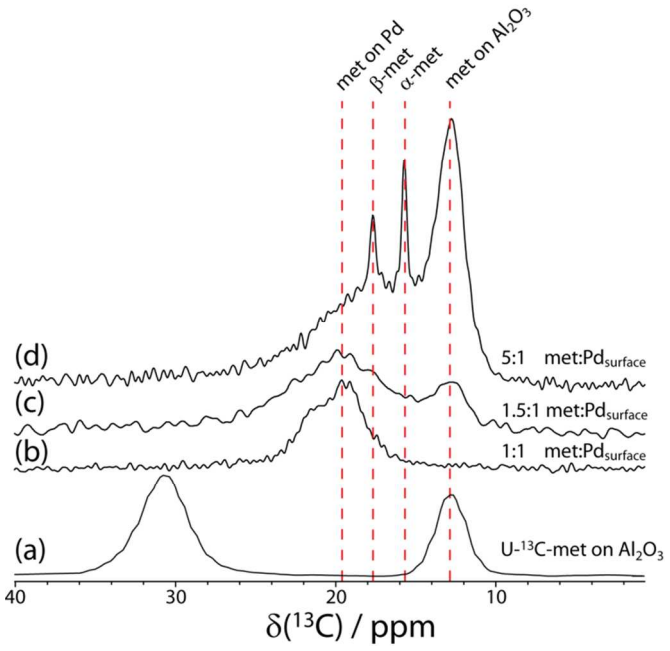

Figure 1. ^{13}C MAS spectra (methyl region) of pure γ-Al_2O_3 impregnated with uniformly ^{13}C-enriched methionine (a) and Pd/γ-Al_2O_3 samples impregnated with selectively ($^{13}CH_3$) enriched methionine (b-d). The methionine-to-surface-Pd ratios are given based on the number of surface Pd sites determined by CO chemisorption studies. An excess of methionine leads to the appearance of the methyl resonance associated with γ-Al_2O_3-bound methionine, while a larger excess leads to the appearance of resonances from the α- and β-polymorphs of crystalline methionine.

DFT calculations. To determine the extent and direction of the differences in ^{13}C shifts associated with methionine binding to Pd, DFT calculations were performed for free methionine and methionine bound to a Pd_{13} cluster. In agreement with previous experimental findings,[22] these calculations predict slight positive shifts of 12 ppm for the methyl and γ-carbon sites while

the other resonances are largely unaffected by the interaction (see Table S2). These calculations, which reproduce the magnitude and direction of the shifts, are thus consistent with our experimental findings as well as our assignment of the shift to a palladium-sulfur interaction. The absence of relativistic corrections in the DFT calculations is responsible for the overestimation of the shift. [23] A similar calculation performed on a Pd_4 cluster yielded the same trends, albeit the use of a larger cluster improved the agreement with the experiment. A Pd sheet was not used due to the inaccuracy of GGA-calculated band gaps and the well-documented impact of the nanoparticle size on the ^{13}C chemical shifts.[22]

XANES. Previous sulfur 2*p* XPS measurements of a methionine-impregnated Pd catalyst showed a shift of the S absorption peak to higher binding energy, when compared to the absorbance for pure methionine, in agreement with S binding to the Pd surface.[6b] Treatment at 353 K in hydrogen and subsequent re-exposure to air led to methionine cleavage and oxidation at the S position, in agreement with previous NMR results.[6b] The structural information afforded by XPS was insufficient to definitely confirm the binding of methionine to Pd; thus, we opted to perform S K-edge XANES measurements, on the same samples as those used for the NMR studies, to probe the S $s \rightarrow p$ electronic transitions that are sensitive to both chemical speciation and S oxidation states.[24,25]

The S K-edge XANES of the methionine-impregnated γ-Al_2O_3 and Pd/γ-Al_2O_3 revealed the various chemical states of S in each sample (see Figure 2a). The peak observed in all spectra around 2472.5 eV is attributed to S-C bonding in the methionine[25] and is less intense in both γ-Al_2O_3 and Pd/γ-Al_2O_3 as a result of the S-to-metal/metal oxide surface binding.[26,27] Notably, the S-C feature for the Pd/γ-Al_2O_3 was also further decreased and shifted towards a higher energy compared to the γ-Al_2O_3, likely as a result of the more intense Pd-S interaction between the

methionine and Pd nanoparticles.[26,27] The bulk PdS sample did not exhibit the S-C feature, although this sample does show an intense pre-edge feature at 2470.5 eV, corresponding to the effect of Pd *d*- and S *p*-orbital hybridization on S $s \rightarrow p$ transitions.[26,27] The γ-Al_2O_3 and Pd/γ-Al_2O_3 samples also exhibit pre-edge features around 2470.5 eV that can be associated with metal-S interactions and correspond to the change in their respective S-C features;[26,27] however, the pre-edge of Pd/γ-Al_2O_3 is much more intense and thus implies a bonding mode that is analogous to Pd-S in bulk PdS. We also note that multiple overlapping pre-edge features are discernible in the spectrum of Pd/γ-Al_2O_3, which are likely a result of Pd-S interactions similar to those in bulk PdS, as well as Pd-S interactions similar to those in metal-thiolate systems.[26,27] Taken together, the pre-edge and main-absorption edge features support that Pd-S bonding is the major component of the stabilization of methionine in Pd/γ-Al_2O_3.

The S K-edge and the corresponding Pd L_3-edge data also allow for a better understanding of the overall reaction mechanism between methionine and the catalyst. In particular, γ-Al_2O_3 exhibits a large feature at 2475.5 eV consistent with methionine sulfoxide,[25] which is known to form when methionine is exposed to air,[28] while Pd/γ-Al_2O_3 does not, and rather, exhibits a large feature at 2481.5 eV consistent with a more oxidized species,[25] which was also indicated by earlier XPS and NMR results. Further to this mechanism, the Pd L_3-edge (which probes Pd $p \rightarrow d$ transitions and is therefore sensitive to the Pd oxidation state,[29,30] see Figure 2b) shows an explicit decrease in the major feature at 3175 eV of Pd/γ-Al_2O_3 upon impregnation with methionine, demonstrating a corresponding partial reduction of Pd and supporting a redox-type reaction between methionine and Pd. Overall, the XANES measurements support that the Pd-S interactions are a major component of the stabilization of the

methionine in Pd/γ-Al_2O_3, as well as demonstrating the oxidative reactions that the methionine undergoes in the presence of Pd.

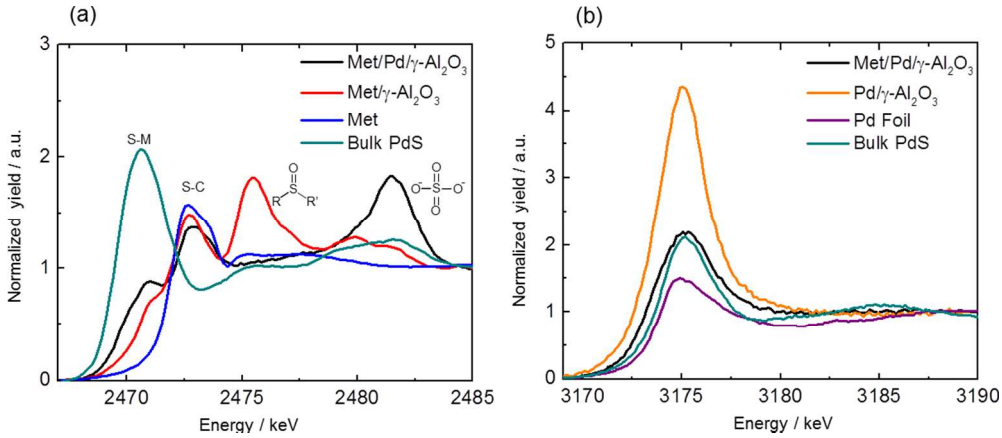

Figure 2. XANES data for γ-Al_2O_3 and Pd/γ-Al_2O_3 catalysts impregnated with methionine, as well as an unreacted Pd/γ-Al_2O_3 catalyst. The S K-edge XANES data in (a) show more intense pre-edge features (~2470.5 eV) and less intense main absorption edge (2472.5 eV) features for the Pd/γ-Al_2O_3, indicating Pd-S bonding. The 2475.5 eV feature reveals the presence of a methionine sulfoxide in the γ-Al_2O_3, while the methionine in the Pd/γ-Al_2O_3 has been converted to a sulfate species, as indicated by the feature at 2481.5 eV. The Pd L_3-edge XANES data in (b) show a decrease in the main absorption at 3175 eV, which correlates to the reduction of the Pd with the addition of methionine.

DNP Performance. The DNP enhancement factors (ε) measured using both ^{13}C CPMAS as well as ^{27}Al PRESTO are tabulated in Table 1. Interestingly, larger enhancement factors were obtained in the absence of Pd nanoparticles, in otherwise identical samples. The reduction in enhancement factors is likely caused either by the magnetism of the Pd nanoparticles, as reported previously,[31] or a partial reflection of the microwaves. The sample temperature was not unusually higher in the presence of Pd, perhaps due to the low metal loading (2%). Nevertheless, large enhancement

factors are obtained in the presence of Pd nanoparticles, permitting a more extensive SSNMR characterization.

Table 1. DNP enhancement factors measured for the different samples

Sample	ε(^{13}C; CPMAS)	ε(^{27}Al; PRESTO-III)
γ-Al_2O_3	-	205
methionine on γ-Al_2O_3	220	232
methionine on Pd/γ-Al_2O_3	67	72
PVA/Pd/γ-Al_2O_3	90	112
methionine on PVA/Pd/γ-Al_2O_3	230[a]	130

[a] This factor corresponds to the enhancement of the solvent (TCE) as the resonances from the sample were too weak to be detected in the absence of microwaves. For PVA/Pd/γ-Al_2O_3 the enhancement factor of the solvent resonance was 162 while that of the sample was only 90.

^{13}C{^{27}Al} RESPDOR. *Experimental approach and data analysis*. To gain a greater insight into the location of the adsorbates at the catalyst surfaces we first attempted to adapt the approaches used for silica materials and perform ^{27}Al{^{1}H} HETCOR experiments. For these experiments, we used a Pd/γ-Al_2O_3 catalyst that was impregnated with natural abundance PVA as a benchmark because this material has a high carbon content (~10% w/w). Unfortunately, the ^{27}Al{^{1}H} HETCOR spectrum does not feature any resonances attributable to the ^{1}H nuclei of the PVA coating. Instead, it is dominated by correlations to physisorbed water, represented by a broad ^{1}H peak centered at ~4.5 ppm (see Figure S2 in Supporting Information).[32] Evidently, the higher-resolution afforded by ^{13}C NMR spectroscopy is needed to identify such intermolecular contacts. We have thus opted to use dipolar recoupling to probe the C-Al proximities directly with high resolution.

Dipolar recoupling experiments for the measurement of internuclear distances between a spin-1/2 nucleus and a quadrupolar nucleus, such as ^{27}Al (spin, $I = 5/2$), have reached a mature state. The most recent of these techniques, namely RESPDOR[33] and low amplitude/low alpha rotational-echo double-resonance (LA-REDOR),[34] enable the facile measurement of distances to quadrupolar nuclei possessing small-to-moderate quadrupolar coupling strengths. The RESPDOR experiment, in particular, has been applied for the measurement of proximities and distances between ^{13}C and ^{27}Al spins in bulk materials where the use of a frequency-splitter is required due to the spins' similar Larmor frequencies.[35]

RESPDOR involves the acquisition of two spin echo datasets in which heteronuclear recoupling is applied at the ^{13}C frequency. In one dataset (S) the ^{27}Al spins are saturated at the midway point, whereas in the reference dataset (S_0) no pulses are applied at the ^{27}Al frequency. The extent of ^{13}C dephasing by the ^{27}Al pulses, which is due to the recoupling of ^{27}Al to the ^{13}C spins, is reported as the normalized difference between the two datasets ($\Delta S/S_0$). Plots of $\Delta S/S_0$ as a function of the recoupling time (t_{rec}) can be fit via a master equation to extract the internuclear distance.[36] For alumina, however, an additional complication occurs due to the simultaneous recoupling of multiple ^{13}C-^{27}Al spin pairs. Luckily, the RESPDOR experiment, which uses heteronuclear zero-quantum recoupling, is not affected by dipolar truncation[37] (similarly to REDOR). The total dephasing for an arbitrary number of ^{27}Al spins can thus be calculated relatively easily using a formalism similar to one proposed earlier for REDOR,[38] leading to the following equation; the derivation of which is detailed in the Supporting Information.

$$\frac{\Delta S}{S_0} = 1 - \frac{f}{4\pi}\int_0^{2\pi}\int_0^{\pi}\int_0^{2\pi}\prod_{i=1}^{n}\left[\begin{array}{l}\frac{1}{6}+\frac{5}{18}\cos\left(\frac{D_i\tau\pi}{2}\sin 2\beta_i \sin\alpha_i\right)\\ +\frac{2}{9}\cos\left(D_i\tau\pi \sin 2\beta_i \sin\alpha_i\right)\\ +\frac{1}{6}\cos\left(\frac{3D_i\tau\pi}{2}\sin 2\beta_i \sin\alpha_i\right)\\ +\frac{1}{9}\cos\left(2D_i\tau\pi \sin 2\beta_i \sin\alpha_i\right)\\ +\frac{1}{18}\cos\left(\frac{5D_i\tau\pi}{2}\sin 2\beta_i \sin\alpha_i\right)\end{array}\right]\sin\beta\, d\alpha\, d\beta\, d\gamma \qquad (1)$$

In this equation a powder average is performed around the orientation of a central C-Al vector whose orientation is described by three Euler angles: α, β, and γ. All other C-Al spin pairs, having dipolar coupling constants of D_i, are related to that orientation; their Euler angles correspond to α_i and β_i, where 'i' is an index identifying a particular spin pair. A scaling factor (f) is included to compensate for incomplete saturation of the ^{27}Al spins.[39] Using this equation, RESPDOR dephasing curves can be calculated in a short period of time for spin systems of arbitrary size. We have confirmed the validity of this equation by comparing it, in the context of REDOR, to the exact numerical result (from SIMPSON[40]) as a function of the relative orientation of the dipolar coupling tensors (see Figure S3 in Supporting Information).

In this work, a model based on the *100* surface of γ-Al_2O_3 was used to approximate the ensemble of ^{13}C-^{27}Al distances found at the surface (see Figure 3).[41] From this model, the values of D_i, α_i, and β_i can be calculated for each spin pair using only the distance between carbon and the central aluminum atom as a variable. This distance is used as a definition of the distance to the alumina surface.

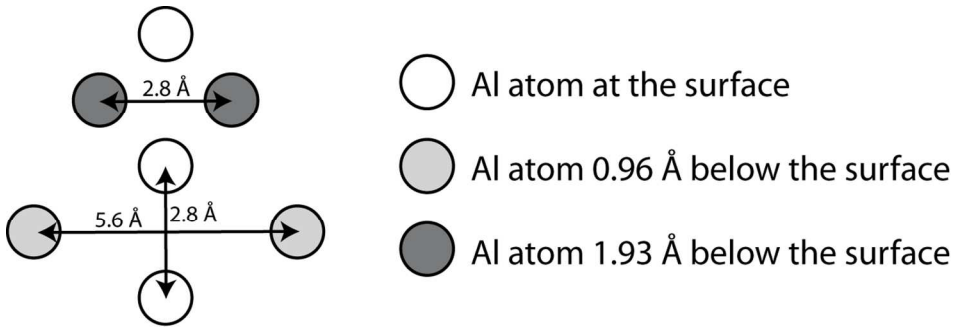

Figure 3. A model of the γ-Al_2O_3 surface used to simulate the $^{13}C\{^{27}Al\}$ RESPDOR curves. Each circle corresponds to an Al atom while the shade indicates the depth of the Al site within the material. The C atom is assumed to be directly above the central Al atom. This C-Al distance is considered to be the distance to the surface.

PVA-Impregnated Pd/γ-Al_2O_3 catalyst. The DNP-enhanced $^{13}C\{^{27}Al\}$ RESPDOR curves for the PVA-impregnated Pd/γ-Al_2O_3 catalyst are shown in Figure 4. Resonances are observed from the PVA coating itself (45 and 64 ppm, labeled A and B in Figure 4), as well as from butyric acid (oxidized solvent from the catalyst preparation method, 184, 39, 19, and 14 ppm; labeled C, D, E and F, respectively) and dehydrated PVA (130 ppm).[6b] All of the resonances were dephased by a ^{13}C-^{27}Al dipolar interaction with the exception of the resonances from the solvent (1,1,2,2-tetrachloroethane, 75 ppm) and from the unsaturated carbon atoms of dehydrated PVA.

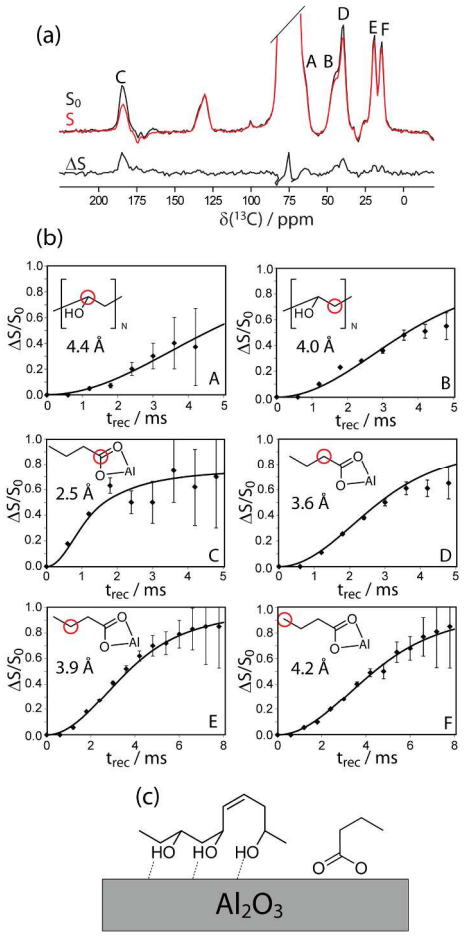

Figure 4. $^{27}Al\{^{13}C\}$ RESPDOR spectra and curves for a Pd/γ-Al_2O_3 catalyst coated with natural abundance PVA. (a) ^{13}C NMR spectra corresponding to the S, S_0, and ΔS signal fractions with a 1.2 ms recoupling time. (b) $\Delta S/S_0$ fractions for individual ^{13}C resonances, error bars correspond to the noise to signal ratios. The best-fit distances to the surface are marked in accordance with the spectra. The conformations solved by RESPDOR are shown in (c).

The C-Al distance measured for the carbonyl of butyric acid (2.5 Å) corresponds to that expected for carbonyl coordinated to a surface aluminum site. The C-Al distances for the remaining carbon atoms increase for carbons C2-C4 in butyric acid (D, E and F, respectively), yet remain sufficiently short (3.6-4.4 Å) to imply that the carbon chain is lying close to the surface (Figure 4c). The measurement of such short distances also suggests that the surface

species have very restricted motions, although the progressive decrease of the dipolar coupling down the chain may be caused by slight librations. Similar distances are observed from the carbon atoms of PVA, indicating that it interacts with the surface by hydrogen bonding interactions rather than by coordination to aluminum. By the same token, when PVA is dehydrated, rendering it void of hydroxyl sites, no interactions to the surface are observed, as evidenced by the lack of dephasing of the peak at 130 ppm. These unsaturated sites are then situated within the pore and away from the support surface. Note that the PVA-surface distances measured here (~4.5 Å) are in perfect agreement with the 5 Å reduction in pore radius measured by N_2 physisorption, suggesting that a monolayer of PVA is formed at the catalyst surface.

Although the RESPDOR data cannot comment on the identity of the aluminum sites that butyric acid is binding, surface-selective DNP-enhanced ^{27}Al PRESTO-III spectra show a relative decrease of the four-coordinate aluminum sites in this sample (Figure S5 in Supporting Information). This finding suggests that butyric acid is coordinating to four-coordinate aluminum surface sites, thus creating new six-coordinate sites.

Methionine-Impregnated γ-Al_2O_3. We have performed similar ^{13}C{^{27}Al} RESPDOR experiments on a γ-Al_2O_3 sample impregnated with methionine to elucidate its interactions with the surface (Figure 5). Resonances corresponding to intact methionine (15, 31, 53 and 180 ppm; labeled A, B, C and D), as well as one representing the carbonate produced by the oxidation of methionine (164 ppm, labeled E), can be observed. All resonances were dephased by an interaction with ^{27}Al. We were, unfortunately, unable to measure a meaningful portion of the dephasing curve for the α-carbon of methionine (C) due to the rapid decay of the signal, likely caused by the strong ^{13}C-^{14}N interaction. Similar to the results obtained with butyric acid, the carbonyl of methionine is coordinated to the alumina surface, as is the carbonate species. We can also conclude that the

chain of methionine is resting prone to the surface, see Figure 5c. The reduced dynamics at low temperature, that likely strengthen the S-Al interactions, may be the cause of the slightly higher methyl chemical shift observed here, when compared to the room temperature data shown in Figure 1. Note that the dipolar dephasing experiments performed on this sample have shown that this chain is far more dynamic at room temperature and thus the prone configuration is likely short-lived at higher temperatures.[6b]

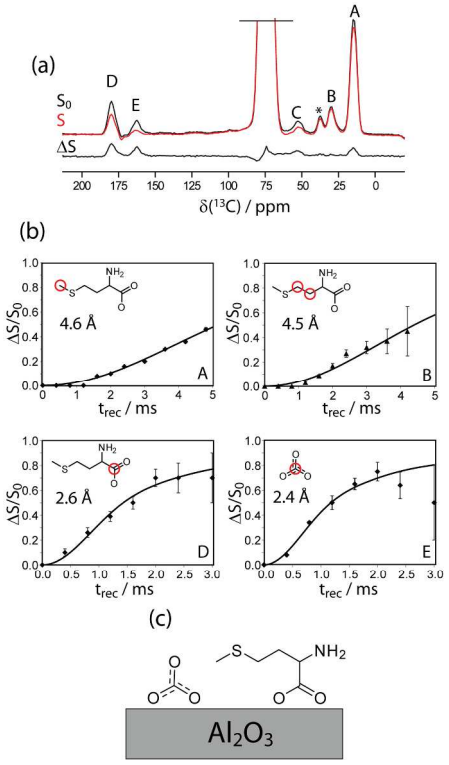

Figure 5. $^{27}Al\{^{13}C\}$ RESPDOR spectra and curves for ^{13}C-enriched methionine adsorbed onto γ-Al_2O_3. (a) ^{13}C NMR spectra, corresponding to the S, S_0, and ΔS signal fractions with a 1.2 ms recoupling time, an asterisk marks the position of a methylene peak from a sulfoxide impurity. (b) $\Delta S/S_0$ fractions for individual ^{13}C resonances, error bars correspond to the noise to signal ratios. The best-fit distances to the surface are marked in accordance with the spectra. The conformations solved by RESPDOR are shown in (c).

Methionine-Impregnated Pd/γ-Al_2O_3. The results of $^{13}C\{^{27}Al\}$ RESPDOR experiments performed on a methionine-impregnated Pd/γ-Al_2O_3 catalyst are shown in Figure 6. Again, all of the resonances from intact methionine (19, 31, 54, and 178 ppm), as well as carbonate, are observed. Surprisingly, the carbon-surface distances determined from RESPDOR signal dephasings are largely unaffected by the presence of the nanoparticles. We can still unambiguously observe that methionine coordinates with the alumina surface through its carbonyl and lies lengthwise on the support surface. These results are particularly interesting given that methionine's coordination to the Pd nanoparticle was confirmed by SSNMR, XPS, and XANES measurements. Taken together, the data show that methionine must be simultaneously coordinating through S to the Pd nanoparticle and through the carboxylate to the alumina support at an interfacial site (Figure 6c). Such interfacial sites are important for many catalytic processes.[42] Note that there is undoubtedly some variability in the carbon-surface distances not reflected by the numbers given in the figure. Remarkably, the interfacially-bound methionine does not degrade in air, which suggests that the interaction with alumina can stabilize methionine against oxidation. The previously-observed oxidation reactions likely occur when methionine reacts at a Pd site situated far from the Al-Pd interface. These reactions lead to previously identified degradation products;[6a] the signals from these low coverage products[6a] were too weak to be detected by RESPDOR.

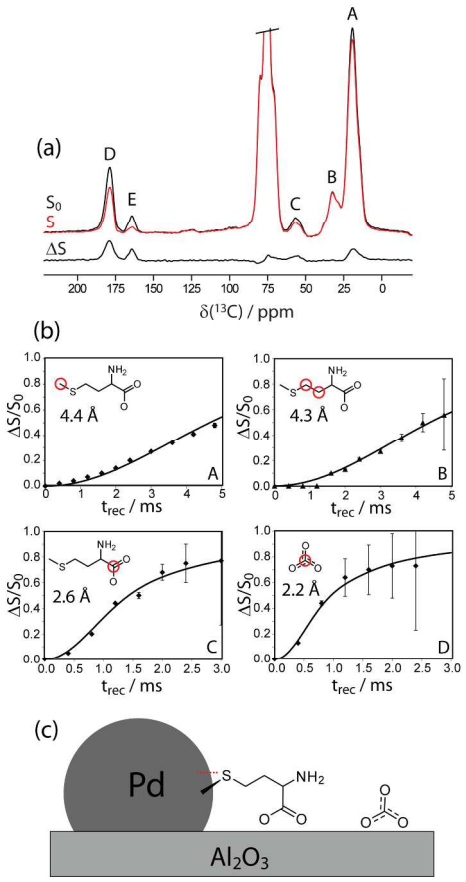

Figure 6. $^{27}Al\{^{13}C\}$ RESPDOR spectra and curves for ^{13}C-enriched methionine adsorbed onto Pd/γ-Al_2O_3. (a) ^{13}C NMR spectra corresponding to the S, S_0, and ΔS signal fractions with a 1.2 ms recoupling time. (b) $\Delta S/S_0$ fractions for individual ^{13}C resonances, error bars correspond to the noise to signal ratios. The best-fit distances to the surface are marked in accordance with the spectra. The conformations solved by RESPDOR are shown in (c).

This level of detail about the behavior of interfacial nanoparticle-support sites in the presence of substrate molecules could not have been obtained by any other means. RESPDOR experiments also show that this coordination is independent of the presence of PVA (see Figure S4 in Supporting Information). We have recently shown that PVA-derived microenvironments stabilize reduced metal catalysts by unfavorably solvating polar species.[43] In the case of

interfacially-bound methionine, the polar group is coordinated to the Al_2O_3 surface, rendering the PVA less effective at preventing the adsorption of these species and potentially providing an explanation for the residual deactivation observed in the previous work in this area.[7]

Conclusions

We have shown that elusive interfacial sites at the surface of γ-Al_2O_3 can be scrutinized by DNP-enhanced $^{13}C\{^{27}Al\}$ RESPDOR experiments. Specifically, we determined the intermolecular interactions between a protective PVA coating with natural ^{13}C abundance and the surface of a Pd/γ-Al_2O_3 catalyst. Furthermore, we discovered that methionine, a commonly encountered inhibitor of reduced metal catalysts, binds to interfacial Pd sites and is stabilized by coordinating to Al_2O_3 through its carbonyl group. This important new methodology can be applied to measure coordination geometries and conformations of other dilute organic species at alumina surfaces, and to establish structure-activity relationships in other industrially-relevant heterogeneous catalyst systems.

Associated Content

Supporting Information

Chemical shift tables, DFT results, numerical validation of equation 5, and supplementary RESPDOR data. This material is available free of charge via the Internet at http://pubs.acs.org.

Author Information

Corresponding Author

M. Pruski: Ames Laboratory, Iowa State University, 230 Spedding Hall, Ames, IA 50011-3020, USA. Phone: +1 515 294 2017; Fax: +1 515 294 4709; E-mail address: mpruski@iastate.edu.

Present Addresses

† Department of Chemical and Biological Engineering, University of Maine, Orono, ME, 04469, USA

Acknowledgement

This research was supported by the U.S. Department of Energy (DOE), Office of Science, Basic Energy Sciences, Materials Science and Engineering Division (DFT calculations) and Division of Chemical Sciences, Geosciences, and Biosciences (SSNMR). F. P. is supported through a Spedding Fellowship funded by the Laboratory Directed Research and Development (LDRD) program at the Ames Laboratory. Ames Laboratory is operated for the DOE by Iowa State University under Contract No. DE-AC02-07CH11358. F. P. thanks NSERC (Natural Sciences and Engineering Research Council of Canada) and the Government of Canada for a Banting Postdoctoral Fellowship. B.H.S. thanks the National Science Foundation Engineering Research Center program (EEC-0813570) for support. J.H.H. thanks the NSERC Discovery Grant program for research support. Support for J.D.P. was provided by National Sciences and Engineering Research Council of Canada (NSERC) and Queen's University. The authors would also like to thank the SXRMB beamline staff at the Canadian Light Source (CLS). The CLS is supported by NSERC, the Canadian Institutes of Health Research, the Province of Saskatchewan, Western Economic Diversification Canada, and the University of Saskatchewan. J.D.P. also acknowledges the receipt of support from the CLS Graduate and Post-Doctoral Student Travel Support Program. T.J.S. acknowledges support from the National Science Foundation Graduate Research Fellowship Program (DGE-1256259).

References

(1) Lesage, A.; Lelli, M.; Gajan, D.; Caporini, M. A.; Vitzthum, V.; Miéville, P.; Alauzun, J.; Roussey, A.; Thieuleux, C.; Mehdi, A.; Bodenhausen, G.; Copéret, C.; Emsley, L. *J. Am. Chem. Soc.* **2010**, *132*, 15459.

(2) Kobayashi, T.; Perras, F. A.; Slowing, I. I.; Sadow, A. D.; Pruski, M. *ACS Catal.* **2015**, *5*, 7055.

(3) (a) Lelli, M.; Gajan, D.; Lesage, A.; Caporini, M. A.; Vitzthum, V.; Miéville, P.; Héroguel, F.; Rascón, F.; Roussey, A.; Thieuleux, C.; Moualleg, M.; Veyre, L.; Bodenhausen, G.; Copéret, C.; Emsley, L. *J. Am. Chem. Soc.* **2011**, *133*, 2104; (b) Samantaray, M. K.; Alauzun, J.; Gajan, D.; Kavitake, S.; Mehdi, A.; Veyre, L.; Lelli, M.; Lesage, A.; Emsley, L.; Copéret, C.; Thieuleux, C. *J. Am. Chem. Soc*. **2013**, *135*, 3193; (c) Conley, M. P.; Drost, R. M.; Baffert, M.; Gajan, D.; Elsevier, C.; Franks, W. T.; Oschkinat, H.; Veyre, L.; Zagdoun, A.; Rossini, A.; Lelli, M.; Lesage, A.; Casano, G.; Ouari, O.; Tordo, P.; Emsley, L.; Copéret, C.; Thieuleux, C. *Chem. Eur. J*. **2013**, *19*, 12234; (d) Grüning, W. R.; Rossini, A. J.; Zagdoun, A.; Gajan, D.; Lesage, A.; Emsley, L.; Copéret, C. *Phys. Chem. Chem. Phys.* **2013**, *15*, 13270; (e) Sangodkar, R. P.; Smith, B. J.; Gajan, D.; Rossini, A. J.; Roberts, L. R.; Funkhouser, G. P.; Lesage, A.; Emsley, L.; Chmelka, B. F. *J. Am. Chem. Soc.* **2015**, *137*, 8096.

(4) (a) Trueba, M.; Trasatti, S. P. *Eur. J. Inorg. Chem.* **2005**, 3393; (b) Rozita, Y.; Brydson, R.; Comyn, T. P.; Scott, A. J.; Hammond, C.; Brown, A.; Chauruka, S.; Hassanpour, A.; Young, N. P.; Kirkland, A. I.; Sawada, H.; Smith, R. I. *ChemCatChem* **2013**, *5*, 2695.

(5) (a) Vitzthum, V.; Miéville P.; Carnevalle, D.; Caporini, M. A.; Gajan, D.; Copéret, C.; Lelli, M.; Zagdoun, A.; Rossini, A. J.; Lesage, A.; Emsley, L.; Bodenhausen, G. *Chem. Commun*.

2012, *48*, 1988; (b) Lee, D.; Takahashi, H.; Thankamony, A. S. L.; Dacquin, J.-P.; Bardet, M.; Lafon, O.; De Paëpe, G. *J. Am. Chem. Soc*. **2012**, *134*, 18491; (c) Lee, D.; Duong, N. T.; Lafon, O.; De Paëpe, G. *J. Phys. Chem. C* **2014**, *118*, 25065; (d) Perras, F. A.; Kobayashi, T.; Pruski, M. *Phys. Chem. Chem. Phys.* **2015**, *17*, 22616.

(6) (a) Johnson, R. L.; Perras, F. A.; Kobayashi, T.; Schwartz, T. J.; Dumesic, J. A.; Shanks, B. H.; Pruski, M. *Chem. Commun*. **2016**, *52*, 1859; (b) Johnson, R. L.; Schwartz, T. J.; Dumesic, J. A.; Schmidt-Rohr, K. *Solid State Nucl. Magn. Reson*. **2015**, *72*, 64.

(7) Schwartz, T. J.; Johnson, R. L.; Cardenas, J.; Okerlund, A.; Da Silva, N. A.; Schmidt-Rohr, K.; Dumesic, J. A. *Angew. Chem. Int. Ed.* **2014**, *53*, 12718.

(8) Ravel, B.; Newville, M. *J. Synchrotron Rad.* **2005**, *12*, 537.

(9) Zagdoun, A.; Casano, G.; Ouari, O.; Schwarzwälder, M.; Rossini, A. J.; Aussenac, F.; Yulikov, M.; Jeschke, G.; Copéret, C.; Lesage, A.; Tordo, P.; Emsley, L. *J. Am. Chem. Soc.* **2013**, *135*, 12790.

(10) Zhao, X.; Hoffbauer, W.; auf der Günne, J.; Levitt, M. H. *Solid State Nucl. Magn. Reson.* **2004**, *26*, 57.

(11) Bielecki, A.; Kolbert, A. C.; Levitt, M. H. *Chem. Phys. Lett*. **1989**, *155*, 341.

(12) Fu, R.; Smith, S. A.; Bodenhausen, G. *Chem. Phys. Lett.* **1997**, *272*, 361.

(13) Lu, X.; Lafon, O.; Trébosc, J.; Tricot, G.; Delevoye, L.; Méar, F.; Montagne, L. Amoureux, J. P. *J. Chem. Phys.* **2012**, *137*, 144201.

(14) (a) Kentgens, A. P. M.; Verhagen, R. *Chem. Phys. Lett*. **1999**, *300*, 435; (b) Perras, F. A.; Viger-Gravel, J.; Burgess, K. M. N.; Bryce, D. L. *Solid State Nucl. Magn. Reson*. **2013**, *51-52*, 1.

(15) (a) Hohenberg, P.; Kohn, W. *Phys. Rev. B* **1964**, *136*, 864; (b) Kohn, W.; Sham, L. J. *Phys. Rev. A* **1965**, *140*, 1133.

(16) Perdew, J. P.; Burke, K.; Ernzerhof, M. *Phys. Rev. Lett.* **1996**, *77*, 3865.

(17) Blöchl, P. E *Phys. Rev. B* **1994**, *50*, 17953.

(18) (a) Kresse, G.; Furthmüller, J. *Phys. Rev. B* **1996**, *54*, 11169; (b) Kresse, G.; Furthmüller, J *Comput. Mater. Sci.* **1996**, *6*, 15.

(19) (a) Pickard, C. J.; Mauri, F. *Phys. Rev. B* **2001**, *63*, 245101; (b) Yates, J. R.; Pickard, C. J.; Mauri, F. *Phys. Rev. B* **2007**, *76*, 024401.

(20) Monkhorst, H. J.; Pack, J. D. *Phys. Rev. B* **1976**, *13*, 5188.

(21) Díaz, L. E.; Morin, F. Mayne. C. L.; Grant, D. M.; Chang, C.-j. *Magn. Reson. Chem.* **1986**, *24*, 167.

(22) (a) Zelakiewicz, B. S.; Lica, G. C.; Deacon, M. L.; Tong, Y. *J. Am. Chem. Soc.* **2004**, *126*, 10053; (b) Zelakiewicz, B. S.; de Dios, A. C.; Tong, Y. *J. Am. Chem. Soc.* **2003**, *125*, 18.

(23) (a) Kaupp, M.; Malkina, O. L.; Malkin, V. G.; Pyykkö, P. *Chem. Eur. J.* **1998**, *4*, 118; (b) Fukawa, S.; Hada, M.; Fukuda, R.; Tanaka, S.; Nakatsuji, H. *J. Comput. Chem.* **2001**, *22*, 528.

(24) Solomon, E. I., Hedman, B., Hodgson, K. O., Dey, A., & Szilagyi, R. K. *Coord. Chem. Rev.* **2005**, *249*, 97.

(25) Jalilehvand, F. *Chem. Soc. Rev.* **2006**, *35*, 1256.

(26) Padmos J. D., Zhang, P. *J. Phys. Chem. C.* **2012**, *116*, 23094.

(27) Lim, J. K.; Kim, I.-H.; Kim, K.-H.; Shin, K. S.; Kang, W.; Choo, J.; Joo, S.-W. *Chem. Phys*. **2006**, *330*, 245.

(28) Harris, J. I. *Methods Enzymol.* **1967**, *11*, 390.

(29) Zhang, P.; Sham, T. K. *Appl. Phys. Lett.* **2002**, *81*, 736.

(30) Zhang, P.; Sham, T. K. *Phys. Rev. Lett.* **2003**, *90*, 245502.

(31) Seehra, M. S.; Rall, J. D.; Liu, J. C.; Roberts, C. B. *Mat. Lett*. **2012**, *68*, 347.

(32) DeCanio, E. C.; Edwards, J. C.; Bruno, J. W. *J. Catal.* **1994**, *148*, 76.

(33) Gan, Z. *Chem. Commun*. **2006**, 4712.

(34) Nimerovsky, E.; Goldbourt, A. *J. Magn. Reson*. **2010**, *206*, 52.

(35) (a) Pourpoint, F.; Trébosc, J.; Gauvin, R. M.; Wang, Q.; Lafon, O.; Deng, F.; Amoureux, J.-P. *ChemPhysChem* **2012**, *13*, 3605; (b) Pourpoint, F.; Thankamony, A. S. L.; Volkringer, C.; Loiseau, T.; Trébosc, J.; Aussenac, F.; Carnevale, D.; Bodenhausen, G.; Vezin, H.; Lafon, O.; Amoureux, J.-P. *Chem. Commun*. **2014**, *50*, 933; (c) Wang, C.; Wang, Q.; Xu, J.; Qi, G.; Gao, P.; Wang, W.; Zou, Y.; Feng, N.; Liu, X.; Deng, F. *Angew. Chem. Int. Ed.* **2016**, *55*, 2507; (d) Huang, M.; Wang, Q.; Yi, X.; Chu, Y.; Dai, W.; Li, L.; Zheng, A.; Deng, F. *Chem. Commun.* **2016**, *52*, 10606.

(36) Chen, L.; Lu, X.; Wang, Q.; Lafon, O.; Trébosc, J.; Deng, F.; Amoureux, J.-P. *J. Magn. Reson*. **2010**, *206*, 269.

(37) Chen, L.; Wang, Q.; Hu, B.; Lafon, O.; Trébosc, J.; Deng, F.; Amoureux, J.-P. *Phys. Chem. Chem. Phys*. **2010**, *12*, 9395.

(38) Goetz, J. M.; Schaefer, J. *J. Magn. Reson.* **1997**, *127*, 147.

(39) Lu, X.; Lafon, O.; Trébosc, J.; Amoureux, J.-P. *J. Magn. Reson.* **2012**, *215*, 34.

(40) Bak, M.; Rasmussen, J. T.; Nielsen, N. C. *J. Magn. Reson.* **2000**, *147*, 296.

(41) Smrčok, Ľ.; Langer, V.; Křesťan, J. *Acta Cryst. Sect. C* **2006**, *62*, i83.

(42) (a) Lu, J.; Elam, J. W.; Stair, P. C. *Acc. Chem. Res.* **2013**, *46*, 1806; (b) Liu, B.; Liu, J.; Li, T.; Zhao, Z.; Gong, X.-Q.; Chen, Y.; Duan, A.; Jiang, G.; Wei, Y. *J. Phys. Chem. C* **2015**, *119*, 12923.

(43) Schwartz, T. J.; Wesley, T. S.; Dumesic, J. A. *Top. Catal.* **2016**, *59*, 19.

TOC graphic